Applied Catalysis B: Environmental 113–114 (2012) 134–140

Contents lists available at SciVerse ScienceDirect

Applied Catalysis B: Environmental

journal homepage: www.elsevier.com/locate/apcatb

High photocatalytic performance of zinc hydroxystannate toward benzene and methyl orange

Yibin Chen[a,b], Danzhen Li[a,*], Miao He[a], Yin Hu[a], Hong Ruan[a], Yangming Lin[a], Junhua Hu[a], Yi Zheng[a], Yu Shao[a]

[a] Research Institute of Photocatalysis, State Key Laboratory Breeding Base of Photocatalysis, Fuzhou University, Fuzhou, Fujian 350002, PR China
[b] Department of Biological and Chemical Engineering, Fuqing Branch of Fujian Normal University, Fuqing, Fujian 350300, PR China

ARTICLE INFO

Article history:
Received 2 August 2011
Received in revised form
11 November 2011
Accepted 20 November 2011
Available online 26 November 2011

Keywords:
$ZnSn(OH)_6$
Photocatalysis
Homogeneous precipitation
Hydrothermal method

ABSTRACT

Two facile and green methods without any templates, catalysts, surfactants or organic solvents were applied to synthesize $ZnSn(OH)_6$ nanoparticles, i.e. homogeneous precipitation (HP) and hydrothermal (HT). The photocatalytic activities were evaluated on the degradation of organic pollutants under ultraviolet light illumination. Compared to commercial P25, the photoactivity of $ZnSn(OH)_6$ was remarkably improved. The conversion and mineralization ratio of the photocatalytic degradation of benzene by the $ZnSn(OH)_6$-HP were up to 75% and 68%, which is about 20 and 2 times higher than that of P25. The $ZnSn(OH)_6$ has also exhibited high performance toward other persistent organic compounds as well as methyl orange in suspended solution. The order of photodegradation efficiencies of different catalysts was $ZnSn(OH)_6$-HP > P25 > $ZnSn(OH)_6$-HT. Based on the characterization results and the detection of active species, the possible mechanism of the high photocatalytic activity of $ZnSn(OH)_6$-HP was discussed. The simplified synthesis of zinc hydroxystannate with outstanding activity could be promisingly used in the future photocatalytic application.

1. Introduction

In recent years, the treatment of persistent organic pollutants (POPs) via green chemical processes has been a very attractive research topic [1]. Among several advanced oxidation technologies have been proposed for POPs removal, semiconductor photocatalysis for the photodegradation of organic pollutants is proved to be the most promising technique [2,3]. It has been shown that many POPs could be efficiently degraded and mineralized into CO_2 and H_2O when the photocatalysts were irradiated by ultraviolet light. However, the accumulation of less-reactive by-products on the photocatalyst surface particularly for the oxidation of aromatics could lead to the deactivation of catalysts [4,5]. It becomes a challenge on the further study of efficient treatment of POPs that persisted in the environment.

Recently, efforts have been made to improve the efficiency of TiO_2 for the photodecomposition of benzene at room temperature by introducing magnetic field [6] or H_2 [7,8] into the photochemical reaction system. However, it is not easy to put such a complicated hybrid system into practice. Other intense research activities have been devoted to the synthesis of new non-titania photocatalysts, such as α-Ga_2O_3 [9], $In(OH)_3$ [10,11], and InOOH [12]. Zinc hydroxystannates ($ZnSn(OH)_6$) is a perovskite-structured hydroxide, with similar structure as $In(OH)_3$ [13]. $ZnSn(OH)_6$ has attracted considerable attentions with its application in high effective flame retardants, due to its environment-friendly and safety [14–16]. Several methods such as co-precipitation [17], hydrothermal [18–20] have been developed to prepare $ZnSn(OH)_6$. Recently, $ZnSn(OH)_6$ prepared by a solvothermal method [21] has been reported to exhibit certain photocatalytic activity for the degradation of benzene under UV light irradiation, but there is organic solvents involved in the synthesis. Since, it has been previously proposed that the synthesis of TiO_2 via different methods could result in the differences of the photocatalytic activity [22–25], thus, it is interesting to explore the facile method of $ZnSn(OH)_6$ preparation with high photocatalytic performance toward POPs.

In this study, we reported the remarkable photocatalytic activity of the zinc hydroxystannates prepared by simple homogeneous precipitation and hydrothermal method without any templates, catalysts, surfactants or organic solvents. The obtained samples were characterized by X-ray diffraction, X-ray photoelectron spectroscopy, N_2 adsorption–desorption, UV-vis diffuse reflectance spectroscopy, photoluminescence and the electron spin resonance techniques. The photocatalytic performance on the

* Corresponding author. Tel.: +86 591 83779256; fax: +86 591 83779256.
E-mail address: dzli@fzu.edu.cn (D. Li).

0926-3373/$ – see front matter © 2011 Elsevier B.V. All rights reserved.
doi:10.1016/j.apcatb.2011.11.030

photo-degradation of benzene, cyclohexane or acetone in O_2 gas stream as well as methyl orange (MO) dyes in suspended solution under UV 254 nm light irradiation were investigated.

2. Experimental

2.1. Preparation of $ZnSn(OH)_6$

All reagents were analytical-grade and used without further purification. The $ZnSn(OH)_6$ was prepared by solution method using $ZnCl_2$ and $SnCl_4{\cdot}5H_2O$ as starting materials. In a common synthesis, equal-volume of 0.6 M NaOH and 0.1 M $ZnCl_2$ aqueous solution was added into subsequently 0.1 M $SnCl_4$ solution with magnetic stirring. The mixed aqueous solution was further treated with following methods.

Homogeneous precipitation synthesis of zinc hydroxystannates (*ZnSn*(*OH*)6-*HP*). The above mixed aqueous solution was stirred for 30 min to obtain the white slurry. Then the slurry was washed repeatedly with distilled water to remove excess salts and separated by centrifugation. The product was finally dried at 80 °C in air.

Hydrothermal synthesis of zinc hydroxystannates (*ZnSn*(*OH*)6-*HT*). 70 mL of the above mixed aqueous solution was put into a 100 mL stainless steel autoclave. The autoclave was sealed and maintained at 160 °C for 24 h, and then cooled down naturally. After that, the white product was centrifuged, washed and dried at 80 °C in air.

2.2. Characterizations

X-ray diffraction (XRD) measurement of the samples was performed on a Bruker D8 Advance X-ray diffractometer with Cu Kα radiation. X-ray photoelectron spectroscopy (XPS) analysis was conducted on an ESCALAB 250 photoelectron spectroscopy (Thermo Fisher Scientific) at 3.0×10^{-10} mbar using Al Kα X-ray beam (1486.6 eV). The scanning electron microscopy (SEM) images were obtained on a JEOL JSM 6700F instrument with an accelerating voltage of 20 kV. The transmission electron microscopy (TEM) images were recorded on a JEOL JEM 2010F microscope working at 200 kV. Nitrogen adsorption–desorption isotherm was collected at 77 K using OMNISORP100CX equipment. The specific surface area was calculated using the Brunauer–Emmett–Teller (BET) method. The sample was degassed at 140 °C and 10^{-6} Torr for 5 h prior to the measurement. UV–vis diffuse reflectance spectrum (DRS) was recorded on a Varian Cary 500 Scan UV-Vis-NIR spectrometer with $BaSO_4$ as the background between 200 and 800 nm. The electron spin resonance (ESR) signals of the radicals spin-trapped by 5,5-dimethyl-L-pyrroline-*n*-oxide (DMPO) were recorded with an EPR spectrometer (ESP 300E, Bruker). A spot UV-light source of Hamamatsu Co. (LC8) (equipped with a 254 nm filter) was used as a photo-excitation light source. The photoluminescence was measured on an Edinburgh FL/FS900 Spectrophotometer (Edinburgh Instruments Ltd., Livingston, U.K.) with a Xe lamp at room temperature.

The terephthalic acid photoluminescence probing technique (TA-PL) [26], which is rapid, sensitive, and specific, and only needs PL instrumentation, has been often used in the detection of •OH radicals [27–29]. The •OH produced in phocatalytic process can react with terephthalic acid to produce a high fluorescent 2-hydroxyterephthalic acid, whose PL peak is at around 430 nm. Due to the peak intensity of 2-hydroxyterephthalic acid is in proportion to the amount of •OH produced in solution, the hydroxyl radicals can be detected indirectly by monitoring the fluorescence intensity changes of photocatalyst/TA solution when the solution was illuminated.

2.3. Measurement of photocatalytic activity

The photocatalytic oxidation of gas pollutants was operated in a tubular quartz microreactor with a continuous-flow mode. The quartz tube reactor loading 0.3 g catalyst (50–70 mesh) was surrounded by four 4 W fluorescent UV bulbs (TUV 4W/G4 T5, Philips, wavelength 254 nm). The temperature of the reaction was controlled at 35 ± 1 °C by an air-cooling system. Diluted benzene, cyclohexane or acetone vapor (at 0 °C, 280 ± 20 ppm) was introduced into the reactor along with a continuous O_2 gas stream at a total flow rate of 20 cm^3 min^{-1}. Prior to irradiation, the adsorption of benzene on the photocatalyst reached equilibrium. The concentrations of organic gas pollutant and product CO_2 were analyzed by an online gas chromatograph (HP6890), equipped with a thermal conductivity detector, a flame ionization detector, and a Porapak R column.

During photoacatalytic degradations of dyes in the liquid phase, 0.08 g catalyst was suspended in 150 mL 20 ppm MO solution in a quartz tube under UV irradiation. Before irradiation, the suspensions were stirred for 1 h in the dark to ensure the establishment of adsorption–desorption equilibrium. 3 mL liquid was taken at a certain time interval during the experiment and centrifuged to remove the catalyst. The filtrates were analyzed on a Varian UV-vis spectrophotometer (Cary-50, Varian Co.).

3. Results and discussion

3.1. Characterization of $ZnSn(OH)_6$ by XRD, BET, and DRS

The XRD patterns of $ZnSn(OH)_6$ synthesized via two different solution methods are shown in Fig. 1. All these diffraction peaks of the $ZnSn(OH)_6$-HP and $ZnSn(OH)_6$-HT were in line with the standard spectrum (JCPDS No. 20-1455). The nine distinctive peaks at 22.92°, 32.80°, 36.78°, 38.57°, 40.31°, 46.88°, 52.83°, 58.34° and 68.11° were matched with the (2 0 0), (2 2 0), (3 1 0), (3 1 1), (2 2 2), (3 3 1), (4 2 0) and (4 4 0) crystal planes of $ZnSn(OH)_6$, respectively. The absence of any other peaks due to impurities indicated the purity of the product. The average particle size of $ZnSn(OH)_6$-HP and $ZnSn(OH)_6$-HT was approximately estimated from the XRD, which was 42.2 nm and 41.5 nm, respectively.

The morphologies of the as-synthesized $ZnSn(OH)_6$-HP were demonstrated in the SEM and TEM images. As shown in Fig. 2, the most of nanoparticles were cubic and the pores were the interspaces among the nanocubes. The representative HRTEM image with some lattice fringes was shown in Fig. 2c. The interlayer spacing of 0.28 nm, 0.26 nm corresponded to the (2 2 0), (3 1 0)

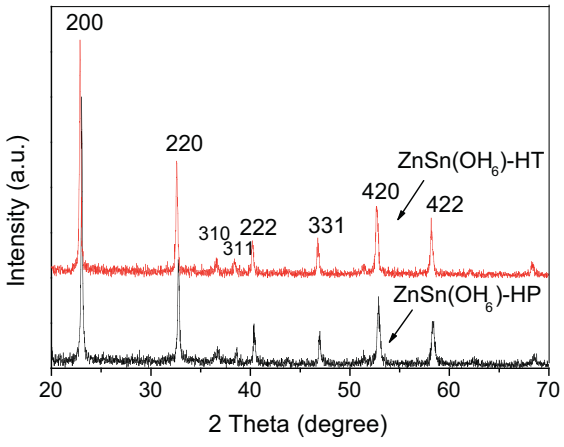

Fig. 1. XRD patterns of the samples prepared via homogenous precipitation and hydrothermal.

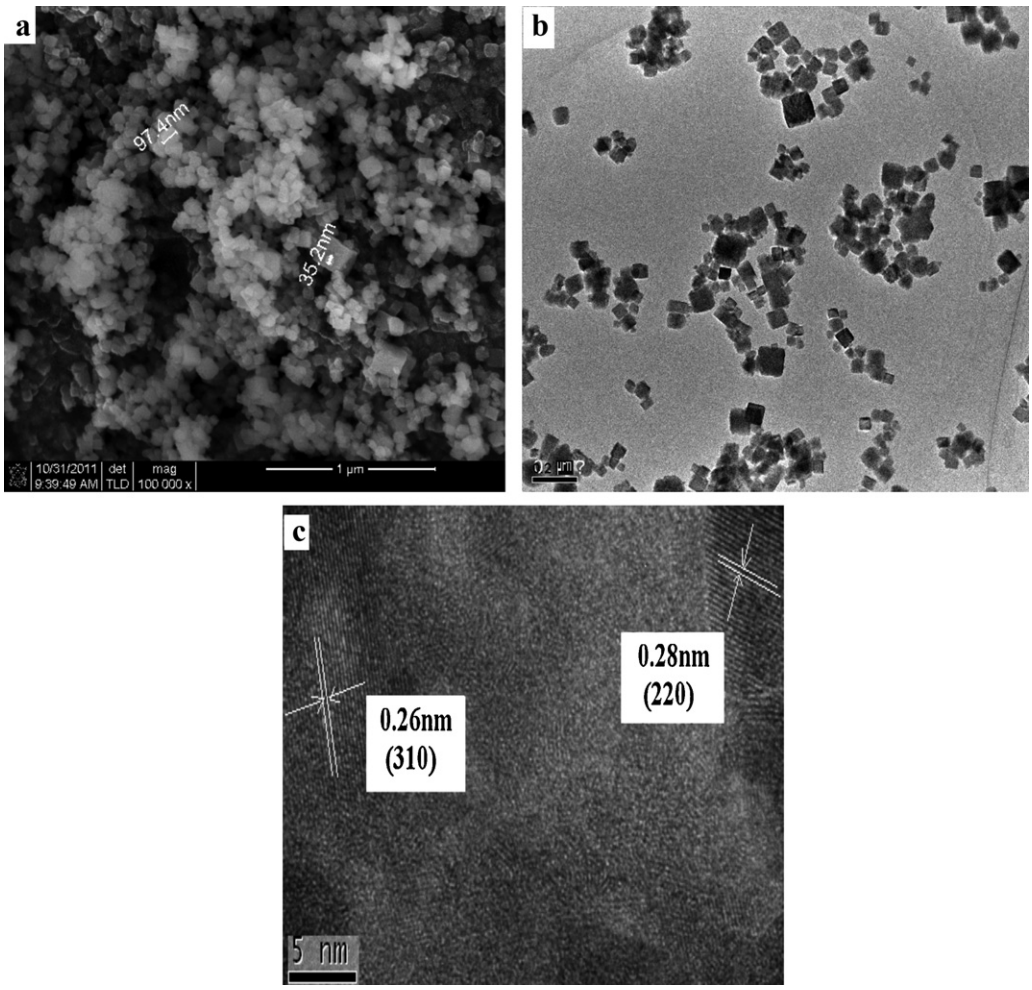

Fig. 2. (a) The SEM image, (b) TEM image and (c) typical HRTEM image of the $ZnSn(OH)_6$-HP nanoparticles.

plane of $ZnSn(OH)_6$, respectively. The size and morphology of the $ZnSn(OH)_6$-HT was shown in Fig. S1.

The N_2-sorption isotherm (Fig. 3) for the as-prepared $ZnSn(OH)_6$ exhibited stepwise adsorption and desorption (type-IV isotherm), indicating that the samples have mesoporous structure [9,30]. The average pore size of the $ZnSn(OH)_6$-HP was 4.0 nm with a narrow distribution of pore size and, whereas that of the $ZnSn(OH)_6$-HT was 40.0 nm. The BET specific surface areas of the $ZnSn(OH)_6$-HP and $ZnSn(OH)_6$-HT, calculated from N_2 isotherms at 77 K, were 71.93 and 31.98 $m^2\,g^{-1}$ respectively.

The UV–vis diffuse reflectance spectra of $ZnSn(OH)_6$ nanoparticles are shown in Fig. 4, which can be seen that the samples show a photo-absorption property in the UV light region. It is well-known that the relation between absorption coefficient and band gap energy of an direct gap semiconductor can be described by the formula

$[F(R)E]^2 = A(E - E_g)$where E and E_g are the photon energy and optical band gap energy, respectively, and A is the characteristic constant of semiconductors [31]. In the equation, $[F(R)E]^2$ has a linear relation with E. Extrapolating the linear relation to $[F(R)E]^2 = 0$ could get the bandgap E_g of the sample. On the basis of this method, the bandgaps of $ZnSn(OH)_6$-HP and $ZnSn(OH)_6$-HT were about 4.35 eV and 3.74 eV, corresponding to the absorption edges were located at 285 nm and 331 nm, respectively.

3.2. Photocatalytic activities of $ZnSn(OH)_6$

The photocatalytic activities of the $ZnSn(OH)_6$ synthesized by the two different methods were evaluated by the degradation of benzene, cyclohexane, acetone and MO under UV-light irradiation. The gas-phase photocatalytic degradation of organic pollutants in a dry O_2 gas stream was carried out under UV light irradiation. Fig. 5 shows that two $ZnSn(OH)_6$ samples present much higher photodegradation activity of benzene than that of P25 under the same conditions. The conversion ratio of benzene on $ZnSn(OH)_6$-HP and $ZnSn(OH)_6$-HT was about 75% and 27%, corresponding to the mineralization ratio was about 68%, 55%, respectively. As to P25, the conversion ratio of benzene was only 5%, and the mineralization ratio was about 24%.

Compared with $ZnSn(OH)_6$-HT and TiO_2, the photoactivity of $ZnSn(OH)_6$-HP was not only much higher but also more stable under UV light irradiation for 36 h. For P25, the amount of product CO_2 was decreased from 40 to 20 ppm, corresponding to the decrease in mineralization of benzene from 55% to 20%. For the $ZnSn(OH)_6$-HT, although the conversion ratio of benzene gradually increased from 20% to 27%, the mineralization of benzene decreased from 80% to 55%. As to $ZnSn(OH)_6$-HP, the conversion of benzene was stable at above 70% and the amount of product CO_2 was up to about 900 ppm, corresponding to the mineralization ratio of benzene of 68%. After a prolonged photocatalytic reaction, only a slight color changing from white to grey yellow was observed for

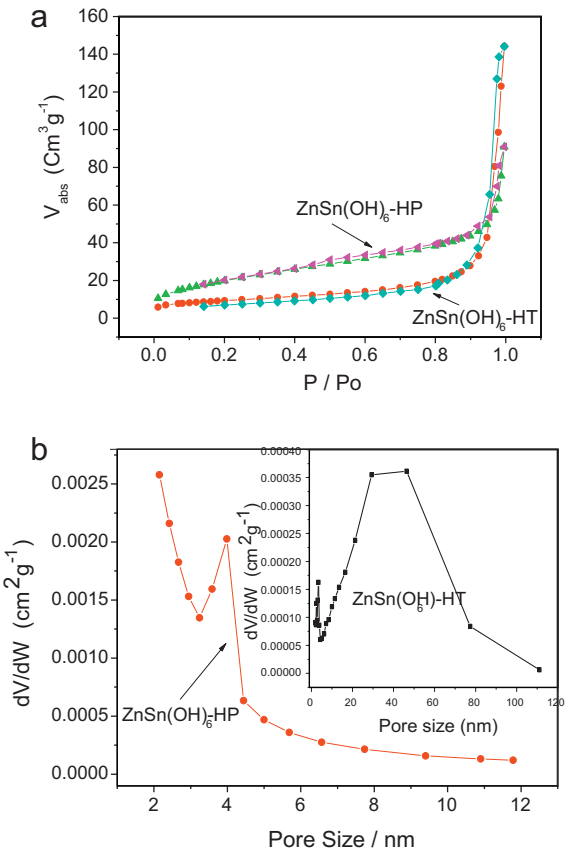

Fig. 3. Nitrogen adsorption–desorption isotherm and the pore size distribution plot for $ZnSn(OH)_6$ The pore size distribution was estimated from the desorption branch of the isotherm.

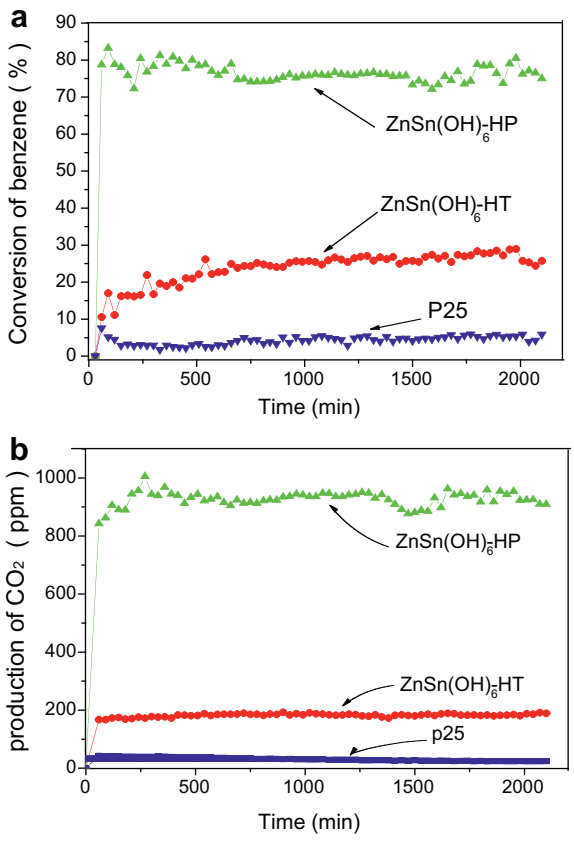

Fig. 5. Conversion of C_6H_6 and the amount of produced CO_2 over the $ZnSn(OH)_6$ as a function of reaction time, with P25-TiO_2 as references.

$ZnSn(OH)_6$-HP, which suggested that only a slightly carbon accumulated on the photocatalyst surface and ensured its high activity and stability.

The experimental data of XPS and XRD on the $ZnSn(OH)_6$-HP before and after reaction demonstrated that the as-prepared photocatalyst was stable (As shown in Fig. S2). The binding energy of Zn, Sn and O in $ZnSn(OH)_6$-HP before and after reaction was nearly the same in the full survey spectrum, only the intensity of the peaks belonged to C1s increased a little after reaction. These suggested that the surface valence states of $ZnSn(OH)_6$ were all stable during the photocatalytic reaction. Furthermore, the XRD patterns of $ZnSn(OH)_6$ before and after reaction also demonstrated that the crystal phase was stable in use. Although the intensity of the patterns after degradation increased a little, the position and the ratio of peaks were nearly the same.

In view of the efficient photocatalytic activity of $ZnSn(OH)_6$ toward benzene, we extended these new photocatalysts for treating other volatile organic compounds. Cyclohexane was choosed as reactant, due to it is not an aromatic organic compound and cannot be sensitized by 254 nm UV light. As shown in Fig. 6, the efficient photo-degradation of cyclohexane on $ZnSn(OH)_6$ was observed. The conversions of cyclohexane on $ZnSn(OH)_6$-HP and $ZnSn(OH)_6$-HT were 23.1% and 8.8%, which is lower than that of benzene, but the mineralizations of cyclohexane on $ZnSn(OH)_6$-HP and $ZnSn(OH)_6$-HT were high up to 94.8% and 74.4%, respectively.

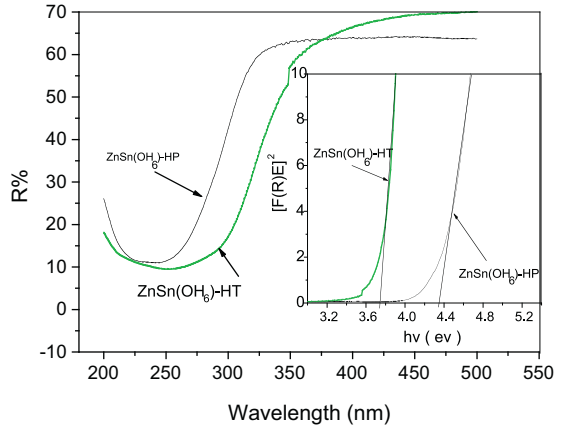

Fig. 4. UV–vis diffuse reflectance spectrum of $ZnSn(OH)_6$ and optical band gap energy (E_g) of $ZnSn(OH)_6$ (inset).

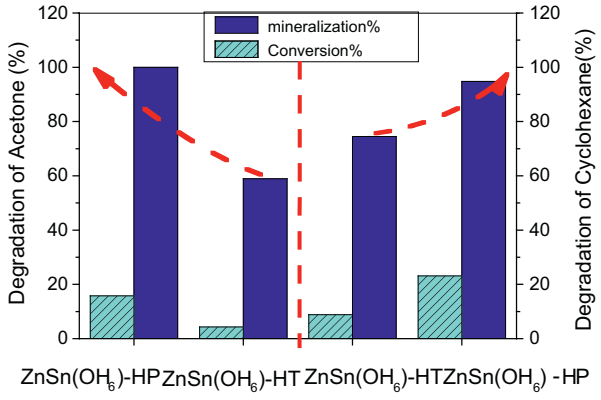

Fig. 6. Photooxidation of different volatile organic pollutants in the presence of $ZnSn(OH)_6$ under UV irradiation.

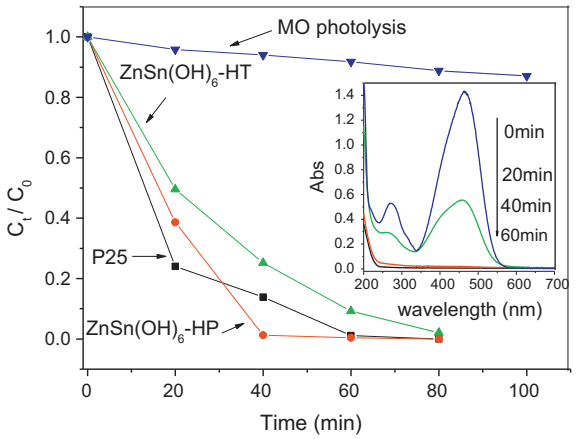

Fig. 7. The photocatalytic activity of $ZnSn(OH)_6$ toward MO with P25 TiO_2 as reference under UV light and time-dependent absorption spectral pattern of MO in the presence of $ZnSn(OH)_6$-HP (inset).

In addition, acetone was chosen in this study since it was detected as an intermediate of benzene photocatalytic degradation reported by Sitkiewitz and Heller [32]. Similar to the cyclohexane, acetone can be photodegradated on $ZnSn(OH)_6$ in O_2 atmosphere. The conversion of acetone over $ZnSn(OH)_6$-HP was 15.8% and that of $ZnSn(OH)_6$-HT was 4.3%, corresponding to the mineralization of acetone over $ZnSn(OH)_6$-HP was 100% and that of $ZnSn(OH)_6$-HT was 58.9%. Obviously, the photocatalytic activities of acetone and cyclohexane on $ZnSn(OH)_6$-HP were also much higher than those of $ZnSn(OH)_6$-HT. The high mineralization ratio of acetone and cyclohexane over $ZnSn(OH)_6$ not only ensured its high and stable photocatalytic activity, but also proved its dependability of photocatalysis.

For photocatalytic reaction in liquid-phase, the $ZnSn(OH)_6$ also showed high photocatalytic activity toward MO in solutions. Fig. 7 displays that the comparison of the photocatalytic efficiency of $ZnSn(OH)_6$ with P25 toward MO during the degradation process. The photocatalytic activity of $ZnSn(OH)_6$-HP was even higher than that of P25, which had been generally recognized as an efficient photocatalyst under UV irradiation. After 40 min irradiation, the decomposition ratio of MO over $ZnSn(OH)_6$-HP and P25 was about 99%, 86%, respectively. Though the photoactivity of $ZnSn(OH)_6$-HT was slightly lower. In the absence of $ZnSn(OH)_6$, only 6% of MO was decomposed by UV light irradiation. Fig. 7 (inset) shows the temporal evolution of the spectral changes of MO solution in the present of $ZnSn(OH)_6$-HP under UV light. With the increase of the illumination time, the absorption peak of MO at 464 nm decreased gradually, and after only 40 min of irradiation, it almost disappeared. In order to contrast their activity preferably, the linear curve fitting of the different photodegradation process was carried through.

Table 1 gives linear regression equations for three catalysts and without catalyst. It was generally suggested that the kinetics of photocatalytic degradation of dyes follows first order kinetics [33,34]. Applying the identical reaction kinetics, the rate constants k (min^{-1}) of photodegradation for MO in present of TiO_2, $ZnSn(OH)_6$-HP, $ZnSn(OH)_6$-HT or non catalyst were calculated to 0.07, 0.101, 0.047, 0.001, respectively. Obviously, the order of photocatalytic degradation efficiencies for MO in liquid phase was $ZnSn(OH)_6$-HP > P25 > $ZnSn(OH)_6$-HT.

Table 1
Linear regression equation of MO (20 ppm) photodegradation using different catalyst under UV 254 light.

Catalysts	Linear regression equation	Correlation coefficient (R)
$ZnSn(OH)_6$-HP	$Ln(C_0/C) = -0.305 + 0.101t$	0.973
$ZnSn(OH)_6$-HT	$Ln(C_0/C) = -0.222 + 0.047t$	0.984
P25	$Ln(C_0/C) = -0.130 + 0.070t$	0.966
No catalyst	$Ln(C_0/C) = -0.007 + 0.001t$	0.996

3.3. Discussions of mechanism

It has been demonstrated that the photocatalytic activity of catalysts depends on its crystal phase, surface area and surface states [35,36]. The overall photocatalytic activity of $ZnSn(OH)_6$-HP was higher than that of $ZnSn(OH)_6$-HT. For example, the conversion of volatile organic pollutant (benzene, cyclohexane, acetone) on $ZnSn(OH)_6$-HP was threefold than that of $ZnSn(OH)_6$-HT. Therefore, it is necessary to explore the impact of the synthesized method on the photocatalytic activity. In general, the overall photocatalytic activity is primarily influenced by three factors: (i) the adsorption ability of the reactants, (ii) the photo-absorption ability in the available light energy region, and (iii) the separation and transporting rate of the photogenerated electrons and holes in the catalyst [37]. First, a large surface area is desirable for strong adsorption of any reactant on the catalyst surface. With a larger surface area of 71.93 $m^2\ g^{-1}$, $ZnSn(OH)_6$-HP has exhibited stronger absorption toward organic pollutant than that of $ZnSn(OH)_6$-HT in the photocatalytic progress. Therefore, it facilitated the pollutants to react with the active species generated on the surface, such as $^{\bullet}OH$ or $O_2^{\bullet -}$, etc. Second, with a wide band gap of 4.35 eV, $ZnSn(OH)_6$-HP owned stronger oxidation potential. The redox ability of the photogenerated holes and electrons generated on $ZnSn(OH)_6$-HP was stronger than that of $ZnSn(OH)_6$-HT. These factors are the decisive reasons that make the overall photocatalytic activity toward organic pollutants (such as benzene, cyclohexane, acetone, MO) of $ZnSn(OH)_6$-HP higher than that of $ZnSn(OH)_6$-HT.

In addition to the large surface area and the wide band gap, the separation and transporting rate of the photogenerated electrons and holes in the catalyst also play important role in the overall catalytic activity of photocatalyst. For the p-block ternary metal oxide semiconductors, the conduction band is usually highly dispersive because of the hybridization of the orbits, which promotes the mobility of the photogenerated electrons, leading to the enhancement of charge separation [38]. Therefore, when the semiconductor $ZnSn(OH)_6$ was irradiated by light with energy larger than its band gap, electron/hole pairs would generated and be effectively separated. And then, The $^{\bullet}OH$ and $O_2^{\bullet -}$ radicals were originated from the reaction of photoinduced electrons (e_{cb}^-) with the absorbed O_2 and the reaction of photogenerated holes (h_{vb}^+) with surface absorptive OH^-, a part of the resulting holes would react with water molecule to produce $^{\bullet}OH$. Therefore, the higher separation and transporting rate of the photogenerated electrons and holes, the higher production of $^{\bullet}OH$ and $O_2^{\bullet -}$, which is the intrinsic reason of the higher photocatalytic activity on $ZnSn(OH)_6$. The contrast of the production of $^{\bullet}OH$ and $O_2^{\bullet -}$ on $ZnSn(OH)_6$-HP and $ZnSn(OH)_6$-HT was carried through.

The generation of $^{\bullet}OH$ radicals was confirmed by terephthalic acid photoluminescence probing technique (TA-PL). The typical photoluminescence (PL) spectra of the $ZnSn(OH)_6$/TA solution was measured at different irradiation time. As shown in Fig. 8a, the fluorescence intensity was increasing steadily with the irradiation time. Fig. 8b shows the temporal changes in fluorescence intensity at 433 nm under UV light (254 nm) irradiation for different synthesized $ZnSn(OH)_6$, and the rate of hydroxyl radical generation for $ZnSn(OH)_6$-HP/TA and $ZnSn(OH)_6$-HT/TA solution was in accordance with the performances of MO degradation, suggesting hydroxyl radicals may be the main reactive species in the solution.

The generation of HO$^{\bullet}$ radicals was also confirmed by the ESR spin-trap with the DMPO technique. As shown in Fig. 8c, four characteristic peaks of the spin adducts DMPO–$^{\bullet}OH$ could be obviously observed in the suspension of $ZnSn(OH)_6$ irradiating by UV light for

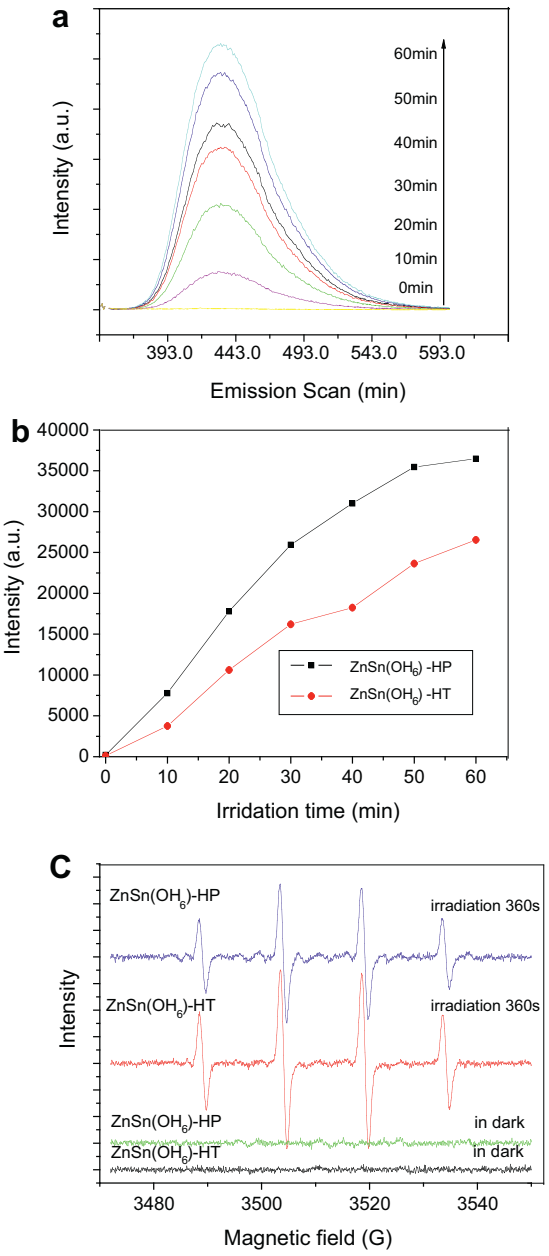

Fig. 8. (a) The temporal changes in fluorescence intensity for $ZnSn(OH)_6$ under UV light (254 nm) irradiation, (b) the comparison of the temporal changes in fluorescence intensity at 433 nm with $ZnSn(OH)_6$ and (c) The ESR signals of the DMPO-•OH in $ZnSn(OH)_6$ system without irradiation and with irradiation for 360 s.

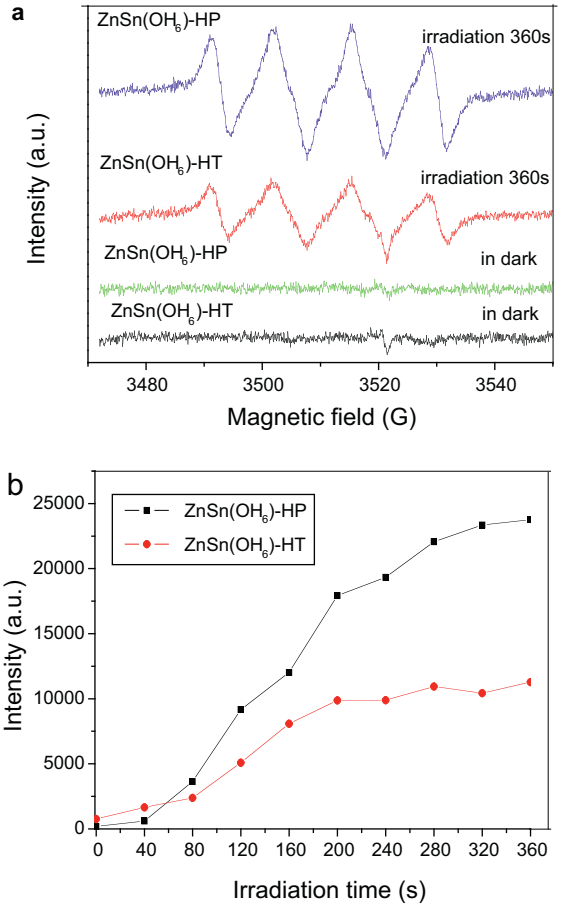

Fig. 9. (a) ESR signals of the DMPO–O_2•⁻ in $ZnSn(OH)_6$ system without irradiation and with irradiation for 360 s and (b) the comparison of the temporal changes in ESR signals of the DMPO–O_2•⁻ in $ZnSn(OH)_6$ system, respectively.

360 s, however in the dark there were no obvious peaks observed. The intensities of DMPO–•OH signals have increased and achieved a steady state for 360 s irradiation, indicating an equilibrium between the production and the extinction of radicals' adducts. This further demonstrated that the •OH is the main reactive species in the photocatalytic process.

The generation of O_2•⁻ radicals was confirmed by the ESR spin-trap with the DMPO technique. As shown in Fig. 9, after irradiation, DMPO–O_2•⁻ adducts with six characteristic peaks could be clearly observed in the methanol solvent, while in dark there were no obvious peaks observed. For $ZnSn(OH)_6$-HT, the intensity of DMPO–O_2•⁻ signal was increasing with the irradiation time and achieved a steady state at 280 s of irradiation, indicating an equilibrium between the production and the extinction of radicals' adducts. For $ZnSn(OH)_6$-HP, the intensity of DMPO–O_2•⁻ signal was always increasing with the irradiation time and no tendency to decay was observed, Until 360 s the DMPO–O_2•⁻ signal intensity of $ZnSn(OH)_6$-HP was greater than that of $ZnSn(OH)_6$-HT, which was in accordance with the performances of benzene degradation in an O_2 gas stream, suggesting O_2•⁻ radicals may be the important reactive species in the photocatalytic degradation of benzene.

The results suggested that the photogenerated charge carriers in both $ZnSn(OH)_6$-HP and $ZnSn(OH)_6$-HT not only possessed strong ability of redox but also long-lived enough to react with the surface-adsorbed hydroxyl group or oxygen. The possible causation is that the conduction band in a ternary wide band gap p-block semiconductor is usually highly dispersive because of the hybridization of the orbital, which promotes the mobility of the photogenerated electrons, leading to the enhancement of charge separation. The difference of photocatalytic activities indicated that photogenerated charge carriers of $ZnSn(OH)_6$-HP would be more easily trapped by the more surface defect sites than $ZnSn(OH)_6$-HT. The enhancement of the separation of electron–hole pair (e^-/h^+) and the generation of •OH and O_2•⁻ radicals are expected in $ZnSn(OH)_6$-HP.

As a ternary wide band gap semiconductor, $ZnSn(OH)_6$ can be efficiently excited to produce electron–hole pairs under UV 254 nm light irradiation. The wide band gap of semiconductor endows the photogenerated holes and electrons with strong redox ability. Especially for $ZnSn(OH)_6$-HP, the larger surface area, the more surface defect sites and the higher mobility of the photogenerated electrons, could result in producing the photo-generated electrons and

holes with longer lifetime to react with adsorbed O_2 and OH^-. By increasing of the formation of $O_2^{\bullet-}$ and $^{\bullet}OH$ radicals, the radical chain reaction is greatly enhanced to react with the absorptive organic pollutants.

4. Conclusions

In present study, the economical and facile solution routes to synthesize $ZnSn(OH)_6$ nanoparticles with high photocatalytic activities toward diverse organic compounds were reported for the first time. The photocatalytic activities of $ZnSn(OH)_6$ toward POPs such as benzene and MO are greatly increased compared to P25. $ZnSn(OH)_6$-HP showed superior performance than $ZnSn(OH)_6$-HT. $ZnSn(OH)_6$-HP with wide band gap, large surface area, high mobility and separated efficiency of the photogenerated carriers, showed remarkable activity on the photocatalytic degradation of organic pollutant.

Acknowledgments

This work was financially supported by the National Natural Science Foundation of China (21173047, 21073036 and 20873023), and National Basic Research Program of China (973 Program, 2010CB234604).

Appendix A. Supplementary data

Supplementary data associated with this article can be found, in the online version, at doi:10.1016/j.apcatb.2011.11.030.

References

[1] B. Meunier, Science 296 (2002) 270–271.
[2] M.R. Hoffmann, S.T. Martin, W. Choi, D.W. Bahnemann, Chem. Rev. 95 (1995) 69–96.
[3] A. Fujishima, T.N. Rao, D.A. Tryk, J. Photochem. Photobiol. C: Photochem. Rev. 1 (2000) 1–21.
[4] R. Mendez-Roman, N. Cardona-Martinez, Catal. Today 40 (1998) 353–365.
[5] G.S. Martra, L. Coluccia, V. Marchese, V. Augugliaro, L. Loddo, M. Palmisano, Catal. Today 53 (1999) 695–702.
[6] W. Zhang, X.X. Wang, X.Z. Fu, Chem. Commun. (2003) 2196–2197.
[7] Y.L. Chen, D.Z. Li, X.C. Wang, X.X. Wang, X.Z. Fu, Chem. Commun. (2004) 2304–2305.
[8] Y.L. Chen, D.Z. Li, X.C. Wang, L. Wu, X.X. Wang, X.Z. Fu, New J. Chem. 29 (2005) 1514–1519.
[9] Y.D. Hou, X.C. Wang, L. Wu, Z.X. Ding, X.Z. Fu, Environ. Sci. Technol. 40 (2006) 5799–5803.
[10] T.J. Yan, J.L. Long, Y.S. Chen, X.X. Wang, D.Z. Li, X.Z. Fu, C. R. Chim. 11 (2008) 101–106.
[11] T.J. Yan, X.X. Wang, J.L. Long, P. Liu, X.L. Fu, G.Y. Zhang, X.Z. Fu, J. Colloid Interface Sci. 325 (2008) 425–431.
[12] Z.H. Li, Z.P. Xie, Y.F. Zhang, L. Wu, X.X. Wang, X.Z. Fu, J. Phys. Chem. C 111 (2007) 18348–18352.
[13] A.N. Christensen, N.C. Broch, O. Heidenstam, A. Nilsson, Acta Chem. Scand. 21 (1967) 1046–1056.
[14] J.Z. Xu, C.Y. Zhang, H.Q. Qu, C.M. Tian, J. Appl. Polym. Sci. 98 (2005) 1469–1475.
[15] F. Andre, P.A. Cusack, A.W. Monk, R. Seangprasertkij, Polym. Degrad. Stab. 40 (1993) 267–273.
[16] P.R. Hornsby, P. Winter, P.A. Cusack, Polym. Degrad. Stab. 44 (1994) 177–184.
[17] L.C. Basciano, R.C. Peterson, P.L. Roeder, I. Swainson, Can. Mineral. 36 (1998) 1203–1210.
[18] Z.G. Lu, Y.G. Tang, Mater. Chem. Phys. 92 (2005) 5–9.
[19] Y.J. Zhang, M. Guo, M. Zhang, C.Y. Yang, T. Ma, X.D. Wang, J. Cryst. Growth 308 (2007) 99–104.
[20] J. Zeng, M.D. Xin, K.W. Li, H. Wang, H. Yan, W.J. Zhang, J. Phys. Chem. C 112 (2008) 4159–4167.
[21] X.L. Fu, X.X. Wang, Z.X. Ding, D.Y.C. Leung, Z.Z. Zhang, J.L. Lomg, W.X. Zhang, Z.H. Li, X.Z. Fu, Appl. Catal. B: Environ. 91 (2009) 67–72.
[22] W. Kongsuebchart, P. Praserthdam, J. Panpranot, A. Sirisuk, P. Supphasrirongjaroen, C. Satayaprasert, J. Cryst. Growth 297 (2006) 234–240.
[23] D.S. Kim, S.Y. Kwak, Appl. Catal. A: Gen. 323 (2007) 110–118.
[24] S. Yuan, Q.R. Sheng, J.L. Zhang, H. Yamashita, D.N. He, Micropor. Mesopor. Mater. 110 (2008) 501–507.
[25] W.J. Zheng, X.D. Liu, Z.Y. Yan, L.J. Zhu, Acs Nano 3 (2009) 115–122.
[26] J.C. Barreto, G.S. Smith, N.H.P. Strobel, P.A. McQuillin, T.A. Miller, J. Life Sci. (1994) 56–61.
[27] K. Ishibashi, A. Fujishima, T. Watanabe, K. Hashimoto, J. Photochem. Photobiol. A: Chem. 134 (2000) 139–142.
[28] T. Hirakawa, Y. Nosaka, Langmuir 18 (2002) 3247–3254.
[29] W. Liu, M. Ji, S. Chen, J. Hazard. Mater. 186 (2011) 2001–2008.
[30] S.J. Gregg, K.S.W. Sing, Adsorption, Surface Area and Porosity, Academic Press, London, 1997, p. 111.
[31] M.A. Butle, J. Appl. Phys. 48 (1977) 1914–1920.
[32] S. Sitkiewitz, A. Heller, New J. Chem. 20 (1996) 233–241.
[33] G.B. Saupe, Y. Zhao, J. Bang, Microchem. J. 81 (2005) 156–162.
[34] C. Zhu, L. Wang, L. Kong, Chemosphere 41 (2000) 303–309.
[35] K. Kato, A. Tsuzuki, H. Taoda, Y. Torii, T. Kato, Y. Butsugan, J. Mater. Sci. 29 (1994) 5911–5915.
[36] R.R. Bacsa, J. Kiwi, Appl. Catal. B: Environ. 16 (1998) 19–29.
[37] W.K. Chang, K.K. Rao, H.C. Kuo, J.F. Cai, M.S. Wong, Appl. Catal. A 321 (2007) 1–6.
[38] Y.F. Liu, X.Q. Liu, Y.S. Shen, Sens. Actuators B 55 (1999) 9–15.